Journal of Inorganic Biochemistry 191 (2019) 60–68

Contents lists available at ScienceDirect

Journal of Inorganic Biochemistry

journal homepage: www.elsevier.com/locate/jinorgbio

Photocytotoxic copper(II) complexes of *N*-salicylyl-L-tryptophan and phenanthroline bases☆

Atrayee Banaspati[a], Dhananjay Das[a], Chandan J. Choudhury[a], Arnab Bhattacharyya[b,*], Tridib K. Goswami[a,*]

[a] Department of Chemistry, Gauhati University, Guwahati 781014, Assam, India
[b] Department of Inorganic and Physical Chemistry, Indian Institute of Science, Bangalore 560012, India

ARTICLE INFO

Keywords:
L-Tryptophan
Salicylaldehyde
Copper
Crystal structure
Photocytotoxicity
Cytosolic localization

ABSTRACT

Four ternary copper(II) complexes of *N*-salicylyl-L-Tryptophan (Sal-TrpH) and phenanthroline bases of general formula [Cu(Sal-Trp)(L)], where L is 1,10-phenanthroline (phen, **1**), dipyrido[3,2-d:2′,3′-f]quinoxaline (dpq, **2**), dipyrido[3,2-a:2′,3′-c]phenazine (dppz, **3**) and 2-(anthracen-1-yl)-1H-imidazo[4,5-f][1,10]phenanthroline (aip, **4**), were synthesized and fully characterized. The complexes were evaluated for their affinity for biomolecules and photocytotoxic activities. Single crystal X-ray diffraction studies of complex **1** revealed that it has a square pyramidal CuN_3O_2 core with the phenolate oxygen of salicylaldehyde occupying the axial coordination site in the solid state. Complexes **1–4** displayed the Cu(II)-Cu(I) redox couples at ~−0.3 V vs. Ag/AgCl reference electrode in DMF-0.1 M $[Bu^n_4N](ClO_4)$. A Cu(II)-based weak d-d band ~650 nm and a moderately strong ligand to metal charge transfer band at ~430 nm were observed in DMF-Tris-HCl buffer (pH 7.2) (1:4 v/v). The complexes are efficient binders to calf thymus DNA and model proteins such as bovine serum albumin and lysozyme. They cleave supercoiled plasmid DNA efficiently when exposed to 446 and 660 nm laser radiation. They are cytotoxic to HeLa (human cervical cancer) and MCF-7 (human breast cancer) cells showing significant enhancement of cytotoxicity upon photo-excitation with low energy visible light. The complexes are found to kill cancer cells through generation of reactive oxygen species (ROS) as confirmed by DCFDA (2′,7′-dichlorofluorescin diacetate) assay. The apoptotic cell death induced by complex **4** was confirmed by Annexin V-Fluorescein isothiocyanate-Propidium iodide assay. Confocal microscopic images using **4** showed its primary cytosolic localization in the HeLa and MCF-7 cells.

1. Introduction

Metal complexes have been extensively investigated for the treatment of various diseases such as cancer, malaria, human immunodeficiency virus, bacterial and fungal diseases etc. among which search for metal-based anticancer agents has received maximum attention [1–10]. Although success of cisplatin and its second generation drugs in clinic triggered extensive research in metal based anticancer agents, severe side effects resulting from poor selectivity and drug-resistance developed by tumors have halted progress in this direction [11,12]. To circumvent these problems enormous efforts have been made in recent times out of which photochemical activation of prodrug, which are otherwise non-toxic to the cells in dark, is the most attractive one [13–17]. Photodynamic activation of prodrugs provides spatiotemporal control over drug action, which is not feasible in case of chemotherapeutic drugs [18]. However, FDA approved porphyrinic photodynamic therapy (PDT) drugs such as Photofrin® has only limited use due to various problems such as poor selectivity, acute allergy and toxic photo-oxidized metabolites generation which causes jaundice [19,20]. Photoactivated chemotherapy (PACT) employing transition metal complexes is a promising alternative as the compounds used are less toxic in dark, selective and releases cytotoxic compounds or radicals only upon excitation with light [21–27]. Sadler and co-workers reported Pt(IV)-azido prodrug which on photo-excitation generates the active compound cisplatin and are active against a number of cell lines in in-vitro studies significantly against cisplatin resistant cell line A2780 [26]. Turro et al. synthesized a number of acetate-bridged di-rhodium complexes that are effective against several cancer cell lines upon photo-irradiation [27]. Photo-induced ligand exchange pathways are proposed to be responsible for their activity in a recent report by the same group [27].

☆ Dedicated to Professor Akhil R. Chakravarty on the occasion of his 65th birthday.

* Corresponding authors.
E-mail addresses: arnab.bhattacharyya1@gmail.com (A. Bhattacharyya), tridibgoswami05@gmail.com (T.K. Goswami).

https://doi.org/10.1016/j.jinorgbio.2018.11.005
Received 9 June 2018; Received in revised form 4 November 2018; Accepted 4 November 2018
Available online 09 November 2018
0162-0134/

Transition metal complexes with redox active metal centers are capable of generation of reactive oxygen species (ROS) through photoredox pathway [28–40]. This offers different mechanism of anticancer activity unlike classical covalent nucleobase binding by Pt(II) complexes. A number of transition metal complexes capable of generating ROS on photoexcitation have been synthesized and evaluated for their anticancer activities in various cancer cell lines [28–42]. A few reports also describe metal complexes capable of formation of both covalent linkages to DNA as well reactive oxygen species thereby showing their activities via dual mechanism of action [41,42]. Copper, being a bio-essential redox active element, could be tailored with suitable ligands to design metal complexes for light activated chemotherapeutic applications [34–40]. Use of functionalized amino acids as ligands could be an interesting strategy to prepare biocompatible transition metal complexes for photodynamic activity [33–37]. As essential nutrients for cells, amino acids have specific sodium dependent active transport systems via membrane-bound transport proteins for their uptake into the cells. This can potentially lead to high and rapid uptake of such compounds into the cells [43]. The ROS generated could potentially damage nucleic acids, proteins, lipids or other vital cellular components in oxidative manner that eventually leads to cell death via apoptotic or necrotic pathway.

Herein, four novel Cu(II) complexes containing a reduced Schiff base derived from salicylaldehyde and L-Tryptophan and phenanthroline bases are studied as visible light induced cytotoxic agents in HeLa (human cervical cancer) and MFC-7 (human breast cancer) cell lines. The synthesis, characterization, DNA and protein binding affinity and photocytotoxic properties of copper(II) complexes, viz. [Cu(Sal-Trp)(L)], where Sal-Trp is *N*-Salicylyl-L-Tryptophan and L is 1,10-phenanthroline (phen in **1**), dipyrido[3,2-d:2′,3′-f]quinoxaline (dpq in **2**), dipyrido[3,2-a:2′,3′-c]phenazine (dppz in **3**) and 2-(anthracen-1-yl)-1H-imidazo[4,5-f][1,10]phenanthroline (aip in **4**) are reported (Chart 1). The choice of L-Tryptophan based ligand is owing to the possible non-covalent interaction of the indole moiety with various biomolecules and its photosensitizing ability. DCFDA (2′,7′-dichlorofluorescin diacetate) assay confirms the generation of ROS on visible light exposure by the complexes. The cell death mechanism induced by complex **4** on exposure to visible light in HeLa cells was found to be of apoptotic nature as confirmed by Annexin V-Fluorescein isothiocyanate-propidium iodide (Annexin V-FITC/PI) assay. Complex **4** with the anthracenyl fluorophore is designed for cellular uptake studies and the confocal microscopic images show significant cytosolic localization of the complex in HeLa and MCF-7cells.

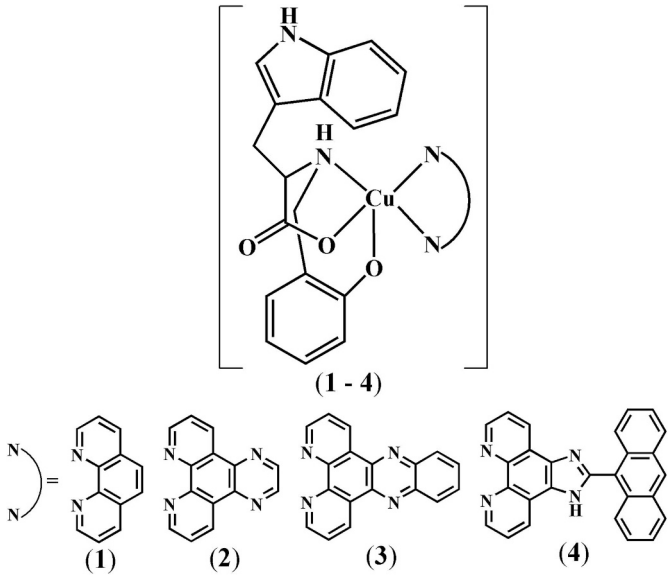

Chart 1. Schematic drawings of the complexes [Cu(Sal-Trp)(L)] (Sal-Trp = *N*-Salicylyl-L-Tryptophan, L = phen, **1**; dpq, **2**; dppz, **3**, nip, **4**) and the heterocyclic bases used.

2. Experimental section

2.1. Materials and measurements

All the reagents and chemicals were obtained from commercial sources (SD Fine Chemicals, India; Loba Chemie, India; Sigma-Aldrich, U.S.A.) and used as such. Tris-(hydroxymethyl)aminomethane-HCl (Tris-HCl) buffer solution was prepared using deionized and sonicated double distilled water. Calf thymus DNA, Dulbecco's Modified Eagle's Medium (DMEM), MTT (3-(4,5-dimethylthiazol-2-yl)-2,5-diphenyltetrazolium bromide), 2′,7′-dichlorofluorescein diacetate (DCFDA), propidium iodide (PI), Dulbecco's phosphate buffered saline (DPBS) and fetal bovine serum (FBS) were purchased from Sigma (U.S.A.). Dipyrido[3,2-d:2′,3′-f]quinoxaline (dpq) and dipyrido[3,2-a:2′,3′-c]phenazine (dppz) were prepared by reported literature procedures using 1,10-phenanthroline-5,6-dione as a precursor reacting with ethylenediamine and 1,2-phenylenediamine, respectively [44,45]. 2-(9-Anthryl)-1*H*-imidazo[4,5-*f*][1,10]phenanthroline (aip) was prepared following literature procedure using 1,10-phenanthroline-5,6-dione and 9-anthraldehyde as precursors [46].

The elemental analysis was carried out using a Thermo Finnigan Flash EA 1112 CHN analyzer. The infrared, UV–visible and emission spectra were recorded on Shimadzu IRAffinity-1S, Shimadzu UV-1800 and Hitachi F-2500 spectrophotometer, respectively. Room-temperature magnetic susceptibility data were obtained from a Sherwood Scientific, Cambridge, England, using $Hg[Co(NCS)_4]$ as a standard. Experimental susceptibility data were corrected for diamagnetic contributions [47]. Cyclic voltammetric measurements were carried out at 25 °C on a CHI660D (CH Instruments, Inc., USA) workstation using a three electrode set-up with a glassy carbon working, platinum wire auxiliary and an Ag/AgCl reference electrode. Tetrabutylammonium perchlorate (TBAP) (0.1 M) was used as a supporting electrolyte in DMF. The electrochemical data were uncorrected for junction potentials. ^{1}H NMR spectra were recorded at room temperature on a Bruker 300 MHz NMR spectrometer. Electrospray ionization mass spectral measurements were done using Agilent 6538 Ultra High Definition Accurate Mass-Q-TOF (LC-HRMS) and Bruker Daltonics make Esquire 300 Plus ESI model mass spectrometers. DNA photocleavage experiments were carried out using continuous-wave lasers from Shanghai Laser and Optics Century Co. Ltd. All cellular experiments requiring light exposure were performed with a broad-band white light using Luzchem Photoreactor (model LZC-1, Ontario, Canada) fitted with eight fluorescent Sylvania white tubes (λ = 400–700 nm, light fluence rate: 2.4 mW cm^{-2}; light dose = 10 J cm^{-2}) and standard protocols. Cytotoxicity data were obtained with a TECAN microplate reader and fitted using GraphPad Prism 6 software. Flow cytometric experiments were performed using fluorescence-activated cell sorting (FACS) Verse instrument (BD Biosciences) fitted with a MoFLo XDP cell sorter and analyzer with three lasers (λ = 488, 365, and 640 nm) and 10-color parameters. Confocal microscopy images were acquired from Leica laser scanning confocal microscope (TCS, SP5 DM6000) with an oil immersion lens with magnification of 63×. Images were processed by using LAS AF Lite software.

2.2. Synthesis

2.2.1. Synthesis of Sal-TrpH

L-Tryptophan (0.4 g, 2.0 mmol) was dissolved in dry methanol (15 mL) by addition of one equivalent NaOH (0.08 g, 2.0 mmol) with continuous stirring. Salicylaldehyde (0.25 mL, 2.0 mmol) was added drop-wise to the above solution. The mixture was refluxed for 1 h, cooled and then treated with an excess of solid $NaBH_4$ in an ice-bath

with constant stirring. After stirring for ~15–20 min the solvent was removed to get a sticky mass which was dissolved in water and treated with dilute HCl to maintain a pH of ~4–5. The ligand which precipitated out as white solid was isolated, thoroughly washed with water and cold methanol and finally dried in vacuum over P_2O_5 (Scheme S1, Supplementary Information). Yield: 0.43 g (~78%).

Anal. Calcd. for $C_{18}H_{18}N_2O_3$: C, 69.66; H, 5.85; N, 9.03. Found: C, 69.38; H, 5.99; N, 9.23. ESI-MS in MeOH: m/z = 311.1606 $[M + H]^+$ (Fig. S1, Supplementary Information). Selected IR data (KBr phase, cm^{-1}): 3428w, 3389w, 3097br, 2755w, 1623vs (COO_{asym}), 1599vs, 1463vs, 1410s (COO_{sym}), 1372s, 12654vs, 1151 m, 1113 m, 1009 m, 946 m, 862 m, 802 m, 749vs, 650 m, 583 m, 523 s (vs, very strong; s, strong; m, medium; w, weak; br, broad). (Fig. S2, Supplementary Information). ^{1}H NMR (D_2O, ppm): δ H^{ind+ph} (6.61–7.53, m, 9H), H^b (3.48, d, 1H, $^3J_{HH}$ = 13.2 Hz), H^c (3.31, m, 2H), $H^{a+a'}$ (2.93, d, 1H, $^3J_{HH}$ = 6.3 Hz) (Fig. S3, Supplementary Information).

2.2.2. Synthesis of [Cu(Sal-Trp)(L)] (L = phen, 1; dpq, 2; dppz, 3; aip, 4)

Complexes **1–4** were prepared by a general synthetic procedure in which a 0.2 g (1.0 mmol) quantity of copper(II) acetate.hydrate in 5 mL of methanol was reacted with methanolic solution of the heterocyclic base (L: phen, 0.19 g; dpq, 0.23 g; dppz, 0.29 g; aip, 0.39 g, 1.0 mmol) while stirring at room temperature for 0.5 h followed by addition of solid Sal-TrpH ligand (1.0 mmol, 0.31 g) in small portions with continuous stirring. The reaction mixture was stirred for another 1 h, and the product was isolated as a green solid in ~85% yield on rotary evaporation followed by washing with cold water and methanol and finally dried under vacuum (yield: 0.44 g, 80% for **1**; 0.49 g, 81% for **2**; 0.58 g, 88% for **3**; 0.64 g 83% for **4**) (Scheme S2, Supplementary Information).

Anal. Calcd. for $C_{30}H_{24}N_4O_3Cu$ (**1**): C, 65.27; H, 4.38; N, 10.15. Found: C, 65.01; H, 4.47; N, 10.25. Selected IR data (KBr phase, cm^{-1}): 3416br, 3208w, 2975w, 2922w, 1615vs (COO_{asym}), 1569s, 1516 m, 1455 m, 1425s (COO_{sym}), 1387 m, 1328 m, 1265 m, 1229 m, 1189 m, 1144 m, 1105 m, 1007 m, 946 m, 878 m, 855 s, 809w, 766 m, 743 s, 718 s, 650 m, 574w, 506 m. ESI-MS in MeOH: m/z = 552.1200 $[M + H]^+$. UV–visible in DMF-Tris-HCl buffer (pH 7.2) (1:4 v/v) [λ_{max}/nm ($\varepsilon/M^{-1}\,cm^{-1}$)]: 675 (70), 415 (330), 271 (22800). μ_{eff} = 1.78 μB at 298 K.

Anal. Calcd. for $C_{32}H_{24}N_6O_3Cu$ (**2**): C, 63.62; H, 4.00; N, 13.91. Found: C, 63.33; H, 4.21; N, 13.77. Selected IR data (KBr phase, cm^{-1}): 3416br, 2975w, 2922w, 1721 m, 1636s (COO_{asym}), 1562s, 1524 m, 1485s, 1463 m, 1412 m (COO_{sym}), 1372 m, 1321w, 1253 m, 1182w, 1129 m, 1083s, 1037w, 1007 m, 931 m, 862 s, 809 m, 764 m, 725 m, 672 m, 620 m. ESI-MS in MeOH: m/z = 604.2984 $[M + H]^+$. UV–visible in DMF-Tris-HCl buffer (pH 7.2) (1:4 v/v) [λ_{max}/nm ($\varepsilon/M^{-1}\,cm^{-1}$)]: 656 (80), 410 (540), 257 (32600). μ_{eff} = 1.81 μB at 298 K.

Anal. Calcd for $C_{36}H_{26}N_6O_3Cu$ (**3**): C, 66.10; H, 4.01; N, 12.85. Found: C, 65.87; H, 4.11; N, 13.02. Selected IR data (KBr phase, cm^{-1}): 3416br, 3226 m, 2914 m, 1638vs (COO_{asym}), 1549 m, 1501s, 1455 m, 1423s (COO_{sym}), 1356 m, 1237 m, 1182 m, 1136 m, 1075s, 1052 m, 1000 m, 923w, 886w, 824 m, 766 s, 725vs, 663 m, 621 m, 566w, 528 m. ESI-MS in MeOH: m/z = 654.1425 $[M + H]^+$. UV–visible in DMF-Tris-HCl buffer (pH 7.2) (1:4 v/v) [λ_{max}/nm ($\varepsilon/M^{-1}\,cm^{-1}$)]: 660 (80), 435 (380), 378 (10800), 360 (12000), 275 (58800). μ_{eff} = 1.79 μB at 298 K.

Anal. Calcd for $C_{45}H_{32}N_6O_3Cu$ (**4**): C, 70.35; H, 4.20; N, 10.94. Found: C, 70.17; H, 4.38; N, 11.12. Selected IR data (KBr phase, cm^{-1}): 3416br, 2975w, 1668s, 1615s (COO_{asym}), 1562vs, 1509 m, 1478 m, 1417 m (COO_{sym}), 1364w, 1296w, 1250 m, 1189w, 1085 m, 1052 m, 1007w, 878 m, 809 m, 725 s, 665 m, 589 m, 506 m. ESI-MS in MeOH: m/z = 768.3803 $[M + H]^+$. UV–visible in DMF-Tris-HCl buffer (pH 7.2) (1:4 v/v) [λ_{max}/nm ($\varepsilon/M^{-1}\,cm^{-1}$)]: 665 (85), 387 (7800), 371 (8400). μ_{eff} = 1.81 μB at 298 K.

2.3. Solubility and stability

The complex **1** was highly soluble in water whereas, complexes **2–4** were sparingly soluble. The complexes were also soluble in MeOH, MeCN, DMF, DMSO and aqueous mixture of the solvents; less soluble in $CHCl_3$ and CH_2Cl_2 and insoluble in hydrocarbon solvents. The stability of the complexes in 20% DMF in phosphate buffer (pH 7.2) was monitored by recording the electronic spectra of the complexes for a period of 24 h at room temperature [48]. There were no significant spectral changes implying that they are quite stable at physiological pH (Fig. S4, Supplementary Information). Comparison of the absorption spectra of the complexes to that of the ligands and metal salt present in their formulations shows that the complexes retain their distinct spectral features indicating that they do not degrade in aqueous buffers (Fig. S5, Supplementary Information). To establish whether the complexes studied remained stable after light irradiation, we also recorded the electronic spectra of the complexes before and after visible light (400–700 nm) irradiation for 1 h. No significant spectral changes were observed suggesting that the complexes are stable under visible light exposed condition (Fig. S6, Supplementary Information).

2.4. X-ray crystallographic procedure

The crystal structure of [Cu(Sal-Trp)(phen)] (**1**) was obtained by single crystal X-ray diffraction method. Crystals of **1** were obtained from the aqueous solution of the complex on slow evaporation of the solvent for several days. Crystal mounting was done on glass fibres with epoxy cement. All geometric and intensity data were collected at room temperature using an automated Bruker SMART APEX CCD diffractometer equipped with a fine focus 1.75 kW sealed tube Mo-K_α X-ray source (λ = 0.71073 Å) with increasing ω (width of 0.3° per frame) at a scan speed of 5 s per frame. Intensity data, collected using an ω-2θ scan mode, were corrected for Lorentz-polarization effects and for absorption [49]. The structure solution was done by the combination of Patterson and Fourier techniques and refined by full-matrix least-squares method using SHELX system of programs [50]. All hydrogen atoms belonging to the complex were in their calculated positions and refined using a riding model. All non-hydrogen atoms were refined anisotropically. The perspective views of the molecules were obtained by ORTEP [51]. Selected crystallographic data are given in Table 1.

2.5. DNA and protein binding experiments

The DNA binding experiments were carried out using calf thymus (ct) DNA by following reported procedures [52]. ct-DNA binding experiments were performed in Tris-HCl buffer at an ambient temperature. In short, concentration of the DNA (in base pairs) was determined by absorption spectroscopy using its molar absorption coefficient value of 6600 $M^{-1}\,cm^{-1}$ at 260 nm. In UV–visible absorption titration experiments, the complex solution (25 μM) in 5 mM Tris-HCl buffer (pH 7.2) containing 20% DMF was titrated with the 210 μM DNA and the intensity of the band at ~260 nm was monitored for the complexes. Due correction was made for the absorption of DNA itself. The spectra were recorded after equilibration for 5 min allowing the complexes to bind to the DNA. The intrinsic equilibrium binding constant (K_b) and the fitting parameter (s) of the complexes to DNA were obtained by McGhee-von Hippel (MvH) method using the expression of Bard and coworkers by measuring the change of the absorption intensity of the spectral bands with increasing concentration of DNA by regression analysis using Eq. (1)

$$(\varepsilon_a - \varepsilon_f)/(\varepsilon_b - \varepsilon_f) = (b - (b^2 - 2K_b{}^2C_t[DNA]_t/s)^{1/2})/2K_bC_t \ldots \quad (1)$$

where $b = 1 + K_bC_t + K_b[DNA]_t/2s$, ε_a is the extinction coefficient observed for the charge transfer absorption band at a given DNA concentration, ε_f is the extinction coefficient of the complex free in solution, ε_b is the extinction coefficient of the complex when fully bound to

Table 1
Selected crystallographic data for the complex [Cu(Sal-Trp)(phen)]·4H_2O (**1**·4H_2O).

Empirical formula	C30 H22 Cu N4 O7
Fw, g M^{-1}	614.06
Crystal system	Hexagonal
Space group	*P*61
a, Å	13.8595(11)
b, Å	13.8595(11)
c, Å	29.625(3)
α, °	90
β, °	90
γ, °	120
V, Å^3	4928.2(10)
Z	6
T, K	296(2)
ρ_{calcd}, g cm^{-3}	1.241
λ, Å (Mo-K_α)	0.71073
μ, cm^{-1}	0.712
Data/restraints/parameters	7151/253/379
F(000)	1890
Goodness-of-fit	0.972
R (F_o)[a], I > 2*σ*(I) [*wR* (F_o)][b]	0.0618 [0.1633]
R (all data) [*wR* (all data)]	0.0857 [0.1784]
Largest diff. peak and hole (e Å^{-3})	0.430, −0.378

[a] $R = \Sigma||F_o| - |F_c|| / \Sigma|F_o|$.
[b] $wR = \{\Sigma[w(F_o^2 - F_c^2)^2] / \Sigma[w(F_o)^2]\}^{1/2}$; $w = [\sigma^2(F_o)^2 + (AP)^2 + BP]^{-1}$, where $P = (F_o^2 + 2F_c^2) / 3$, A = 0.1189; B = 0.

DNA, K_b is the equilibrium binding constant, C_t is the total metal complex concentration, $[DNA]_t$ is the DNA concentration in nucleotides and *s* as the fitting parameter gives an estimate of the binding site size in base pairs [53]. The non-linear least-squares analysis was done using OriginPro 8.

The protein binding study was carried out by tryptophan fluorescence quenching experiments using bovine serum albumin (BSA, 2 μM) or hen egg lysozyme (Lys, 2 μM) in Tris-HCl buffer (pH 7.2). Quenching of the emission intensity of tryptophan residues (Trp 134 and Trp 214) of BSA at 340 nm (excitation wavelength at 280 nm) was monitored using complexes **1–4** as quenchers with increasing concentration [54]. I_0/I vs. [complex] plots were constructed. Linear fit of the data using the equation $I_0/I = 1 + K[Q]$, where I_0 and I are the emission intensity of BSA or lysozyme in the absence of quencher and emission intensity of BSA or lysozyme in the presence of the quencher of concentration [Q] gave the binding constant K (K_{BSA} or K_{Lys}) values using OriginPro 8.

2.6. DNA cleavage experiments

The photocleavage of supercoiled pUC19 DNA (Plasmid, University of California, 30 μM, 0.2 μg, 2686 base pairs) by the complexes **1–4** (10 μM) was studied by agarose gel electrophoresis using in 50 mM tris (hydroxymethyl)methane-HCl (Tris-HCl) buffer (pH 7.2) containing 50 mM NaCl. The DNA photocleavage reactions were performed using a 446 nm blue laser light source [Model no. BLM442TA-100 of LASER CENTURY, Shanghai Laser and Optics Century Co. Ltd., Continuous-Wave (CW), beam diameter 1 × 3 mm and beam divergence 1 × 0.5 mrad, output power 100 mW] and a 660 nm red laser light source [Model no. of RLM20-660D-100, Continuous-Wave (CW), beam diameter (@5 m) ~5 × 7 mm and beam divergence < 0.5 mrad, output power 100 mW] respectively. The samples were incubated for 1 h at 37 °C after light exposure and analyzed for the photo-cleaved products using agarose gel electrophoresis following literature procedures [55,56]. The extent of DNA cleavage was calculated from the intensities of the bands using UVITEC Gel Documentation System. The concentrations of the complexes and additives corresponded to that in the 20 μL final volume of the sample using Tris-HCl buffer.

2.7. Cell viability assay

HeLa (human cervical carcinoma) and MCF-7 (human breast adenocarcinoma) cells were maintained in Dulbecco's Modified Eagle's Medium (DMEM), supplemented with 10% fetal bovine serum (FBS), 100 IU/mL of penicillin, 100 μg/mL of streptomycin and 2 mM Glutamax at 37 °C in a humidified 5% CO_2 incubator. The adherent cultures were grown as monolayer and were passaged once in 4–5 days by trypsinizing with 0.25% Trypsin-EDTA. The photocytotoxicity of the complexes was assessed using MTT assay based on the ability of mitochondrial dehydrogenases in the viable cells to cleave the tetrazolium rings of MTT and forming dark blue membrane impermeable crystals of formazan that were measured at 540 nm giving an estimate of the number of viable cells [57]. Approximately, 1×10^4 cells of HeLa and MCF-7 were plated in a 96-well culture plate in DMEM supplemented with 10% fetal bovine serum and cultured overnight. Different concentrations of the complexes **1–4** were added to the cells, and incubation was continued for 4 h in dark. After incubation, the medium was replaced with 50 mM phosphate buffer, pH 7.4, containing 150 mM NaCl (PBS) and photo-irradiation was done for 1 h in visible light of 400–700 nm using Luzchem Photoreactor (Model LZC-1, Ontario, Canada; light fluence rate: 2.4 mW cm^{-2}; light dose = 10 *J* cm^{-2}). PBS was replaced with 10% DMEM after irradiation. Incubation was continued for a further period of 19 h in dark for light exposed cells and for 20 h in dark for light unexposed cells followed by addition of 25 μL of 4 mg mL^{-1} of MTT to each well and incubated for an additional 3 h. The culture medium was discarded and a 100 μL volume of DMSO was added to dissolve the formazan crystals. The absorbance at 540 nm was determined using an ELISA microplate reader (Bio-Rad, Hercules, CA, USA). The cytotoxicity of the test compounds was measured as the percentage ratio of the absorbance of the treated cells over the untreated controls. The IC_{50} values were determined by nonlinear regression analysis (GraphPad Prism, version 6).

2.8. Partition coefficient of the complexes between n-octanol and water

The partition coefficients of the complexes between *n*-octanol and water were determined experimentally using a modified shake-flask method following reported literature [58]. In short, 4 mL solution of complexes **1–4** in octanol saturated water was shaken with 4 mL of water saturated *n*-octanol in a falcon tube for ~15–20 min using a vortex. The biphasic mixture was centrifuged for ~5 min at 3000 rpm and the layers were separated. The concentration of the **1–4** in each layer was measured spectrophotometrically. The partition coefficients of **1–4** were determined at three different concentrations and averaged out.

2.9. DCFDA assay for detection of ROS

The DCFDA assay was performed to detect the generation of cellular reactive oxygen species (ROS) following the protocols reported by E. Eruslanov and S. Kusmartsev [59]. For flow cytometric analysis for the detection of ROS, ~1×10^6 HeLa cells were seeded, cultured and then incubated with the complexes **1–4** (3 μM). The media was then discarded and the cells were harvested by trypsinization and a single cell suspension in PBS was made. The cells were then treated with 10 μM DCFDA solution (in DMSO) in dark for 30 min at room temperature. Excess media was discarded again and cell suspensions were then further incubated for 1 h in dark or irradiated with visible light source of 400–700 nm (10 J cm^{-2}) to follow the effect of complexes on DCFDA inside cancer cells. The distribution of DCFDA stained HeLa cells was then determined directly by flow cytometry in the FL-1 channel without any further washing.

2.10. Annexin V-FITC-PI assay for apoptosis

Annexin V/FITC/PI assay was carried out for complex **4** (3 μM) in 1% DMSO/DMEM [60]. Approximately 4×10^5 HeLa cells were seeded in six-well plates and cultured for overnight. The cells were incubated with the complex for 4 h in the dark and then exposed to light (1 h, λ = 400–700 nm, light dose = 10 J cm^{-2}) in phenol red free media or kept in dark. Cells were then kept for another 19 h and 20 h respectively for the light exposed and unexposed plates in DMEM-10% fetal bovine serum (FBS) buffer in the dark, after which the medium was discarded, and the cells were trypsinized and re-suspended in 140 μL Annexin V binding buffer (100 mM HEPES/NaOH, pH 7.4 containing 140 mM NaCl and 2.5 mM $CaCl_2$). Annexin-V/FITC (0.5 mL) and propidium iodide (PI; 1 mL) were added to the cell suspensions and incubated for 5 min. Readings were taken with the FACS instrument.

2.11. Confocal microscopy

HeLa and MCF-7 ($\sim 4 \times 10^4$) cells, plated on cover slips, were incubated with 5 μM of complex **4** for 4 h in dark, fixed with 4% paraformaldehyde for 10 min at room temperature and washed with PBS [61]. This was followed by incubation with PI staining solution (50 μg/mL RNase A, 20 μg/mL PI in PBS) for 1 h at 37 °C. The cells were washed free of excess PI and mounted. Images were acquired using the confocal scanning microscope (Leica, TCS SP5 DM6000) and analyzed using the LAS AF Lite software.

3. Results and discussion

3.1. Synthesis and general aspects

Ternary copper(II) complexes [Cu(Sal-Trp)(L)] (**1–4**) having *N*-Salicylyl-L-Tryptophan (Sal-TrpH) and *N*,*N*-donor heterocyclic bases (L: phen, **1**; dpq, **2**; dppz, **3**; aip, **4**) were designed and prepared in good yield (~85%) from the reaction of Sal-TrpH ligand with copper(II) acetate monohydrate and the respective phenanthroline bases in methanol (Chart 1). The imine bond of the Schiff base ligand was reduced to ensure that the complexes do not suffer from the hydrolytic instability in biological fluid [62]. The phenanthroline bases are efficient binders to biomolecules such as DNA and proteins and also result in optimum lipophilicity to the compounds [63]. The complexes were characterized by various spectroscopic and analytical techniques. Selected physicochemical data are given in Table 2. The stability of the complexes **1–4** in solution phase was evidenced from their ESI-MS spectra showing essentially the molecular ion peak as $[M + H]^+$ in methanol (Figs. S7–S10, Supplementary Information). The IR spectra of the complexes displayed characteristic stretching bands at ~1615–1630 cm^{-1} and ~1400–1425 cm^{-1} due to asymmetric and symmetric COO stretch respectively, whereas the free ligand Sal-TrpH showed these bands at ~1620 cm^{-1} and ~1450 cm^{-1} respectively (Figs. S11–S14, Supplementary Information). Magnetic moment values of ~1.8 μ_B at 25 °C suggested the presence of a one-electron paramagnetic $3d^9$-Cu(II) center in the complexes. The UV–visible spectra of **1–4**, recorded in DMF-Tris-HCl buffer (pH 7.2) (1:4 v/v), displayed a broad and weak copper-centered d-d band in the range of 650–680 nm (Fig. 1). A moderately intense ligand to metal charge transfer band was observed ~400 nm in **1–4** [64]. The ligand-centered electronic transitions were observed in the UV region. Complex **4** exhibited an emission spectral band at 468 nm on excitation at 370 nm in DMF at 25 °C (Fig. S15, Supplementary Information). The emissive property of this complex was used for cellular imaging by confocal microscopy. Complexes **1–3** showed quasi-reversible cyclic voltammetric responses in DMF-0.1 M TBAP ~ −0.3 V due to the Cu(II)-Cu(I) couple, whereas complex **4** displayed irreversible response for Cu(II)-Cu(I) couple with very large ΔE_p value of 354 mV (Fig. 1, Fig. S16, Supplementary Information).

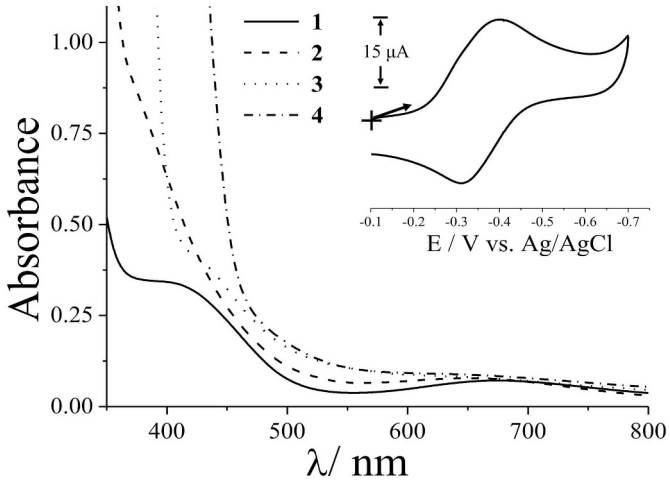

Fig. 1. The electronic spectra of [Cu(Sal-Trp)(phen)] (**1**, —); [Cu(Sal-Trp)(dpq)] (**2**, ——); [Cu(Sal-Trp)(dppz)] (**3**, ····) and [Cu(Ph-Trp)(aip)] (**4**, -·-·) (1 mM) in DMF-Tris-HCl buffer (pH 7.2) (1:4 v/v). The inset shows the cyclic voltammogram of **1** (—) in DMF-0.1 M TBAP.

3.2. Crystal structure

Complex **1** was structurally characterized by single crystal X-ray diffraction method. Complex **1** crystallized in the *P*61 space group of the hexagonal crystal system with six molecules in the unit cell (Fig. S17, Supplementary Information). The ORTEP view of the complex is shown in Fig. 2. Important crystallographic parameters and selected bond distance and angle data are given in Table 1 and Table S1 (Supplementary Information) respectively. The structure of **1** consists of a discrete complex having Cu(II) as the central metal atom. Cu(II)

Table 2
Selected physicochemical data for the complexes [Cu(Sal-Trp)(L)] (L = phen, **1**; dpq, **2**; dppz, **3**; aip, **4**).

Complex	IR/cm^{-1} [$\nu(COO_{asym}; COO_{sym}$][a]	λ_{max}/nm (ε / M^{-1} cm^{-1})[b]	E_f / V (ΔE_p / mV)[c]	μ_{eff}[d] / μ_B	Log$P_{o/w}$
			Cu(II)-Cu(I)		
1	1615; 1406	675 (70), 415 (330)	−0.35 (80)	1.78	−0.468
2	1630; 1406	656 (80), 410 (540)	−0.27 (86)	1.81	0.412
3	1630; 1416	660 (80), 435 (380)	−0.31 (91)	1.79	0.712
4	1622; 1409	665 (85)	−0.28 (354)	1.81	1.02

[a] In KBr phase.
[b] In DMF-Tris-HCl buffer (pH 7.2) (1:4 v/v).
[c] Cu(II)-Cu(I) couple in DMF-0.1 M TBAP, $E_f = 0.5(E_{pa} + E_{pc})$, $\Delta E_p = (E_{pa} - E_{pc})$, where E_{pa} and E_{pc} are the anodic and cathodic peak potentials, respectively. The potentials are vs. Ag/AgCl electrode. Scan rate = 50 mV s^{-1}.
[d] Magnetic moment at 298 K.

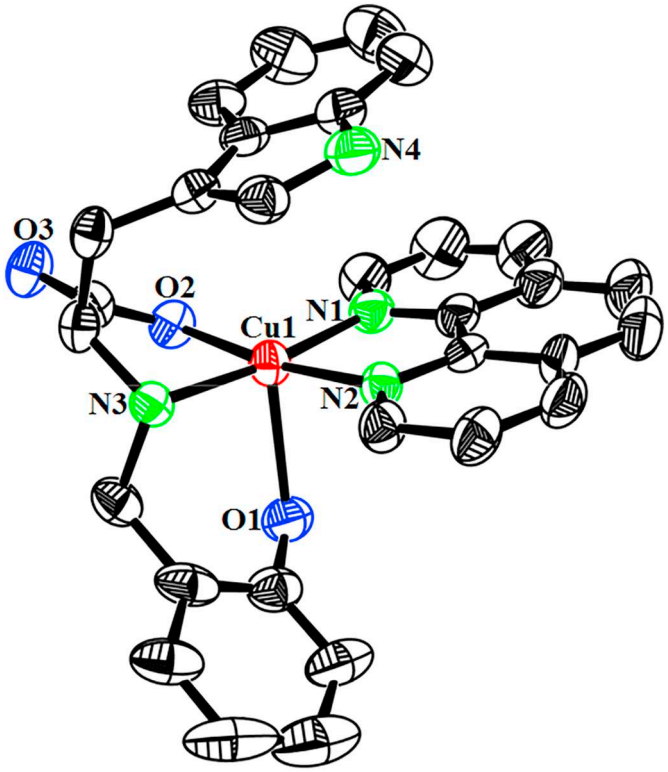

Fig. 2. An ORTEP view of the neutral complex [Cu(Sal-Trp)(phen)] (**1**) showing 50% probability thermal ellipsoids and the atom numbering scheme for the metal and hetero atoms. The hydrogen atoms are omitted for clarity. Atoms color code: Cu, red; O, blue; N, green; C, black. (For interpretation of the references to color in this figure legend, the reader is referred to the web version of this article.)

exhibits a slightly distorted square-pyramidal CuN_3O_2 geometry (degree of trigonality, $\tau = 0.013$). The Sal-Trp ligand provides tridentate NOO coordination to Cu(II) center whereas, the phenanthroline base coordinates in bidentate fashion with the Cu—N bond distances in the range 1.981(6) to 2.015(5) Å. The equatorial and axial Cu—O bond distances are 1.952(5) and 2.325(6) Å, respectively. The chiral carbon of L-Tryptophan has "*S*"-configuration.

3.3. DNA and protein binding property

The affinity of the complexes to bind to calf-thymus (ct) DNA was assessed using UV–visible spectroscopy. UV–visible absorption titration method was used to determine the intrinsic DNA binding constant (K_b) of the complexes by monitoring the change in the absorption intensity of the ligand-centered band of the complexes **1–4** at ~270 nm. Significant hypochromicity with minor bathochromic shift suggests primarily groove binding mode of the complexes to ct DNA in Tris-HCl buffer medium (Fig. S18, Supplementary Information). Classical DNA intercalators that π- stack between two DNA base pairs cause much larger hypochromicity and significant bathochromic shift of the spectral bands [65]. McGhee and von Hippel method was used to evaluate the K_b values of the complexes which range within $(2.40 \pm 0.29) \times 10^5$ to $(6.38 \pm 0.18) \times 10^5\ M^{-1}$ giving the DNA binding affinity order as: **3** > **4** > **2** > **1** (Table S2, Supplementary Information). The complex **3** and **4** having the extended aromatic phenazine ring probably facilitates partial intercalation of this complex through the DNA groove resulting in its higher binding strength compared to their phenanthroline or dipyridoquinoxaline analogues **1** and **2**.

The binding propensity of the complexes **1–4** for bovine serum albumin (BSA) or hen egg lysozyme was evaluated by tryptophan emission-quenching experiment [37,54]. The intensity of emission of the proteins at ~340 nm was found to be quenched gradually with increasing concentration of the complexes **1–4** due to their interaction with the protein molecules in the ground state via static quenching (Figs. S19 and S20, Supplementary Information). A linear plot of I_0/I vs. [complex] gives the K_{BSA} and K_{LYS} values with an order **4** > **3** > **2** > **1** and **3** > **4** > **2** > **1** respectively (Table S2, Supplementary Information). The higher binding affinity of **3** and **4** is probably due to the presence of the largely hydrophobic ligands dppz or aip which fits well to the hydrophobic pockets of the proteins efficiently. The complexes are also found to have higher binding affinity for the extracellular model protein BSA compared to the intracellular protein lysozyme. Therefore, human serum albumin could potentially serve as carrier protein for this kind of metal complexes [66,67].

3.4. Photoinduced DNA cleavage study

The ability of the complexes **1–4** to cleave super-coiled (SC) pUC19 DNA (30 μM, 0.2 μg) to its nicked circular (NC) form in Tris-HCl/NaCl (50 mM, pH 7.2) buffer on irradiation with monochromatic blue and red laser light of wavelengths 446 and 660 nm (laser power = 100 mW) was evaluated using agarose gel electrophoresis. The wavelengths of laser light were chosen based on the electronic absorption spectra of the complexes. The complexes having DNA binding moieties in their formulations were found to be efficient photo-cleavers of SC DNA (Fig. S21, Supplementary Information). The complexes **3** and **4** almost completely convert SC DNA to its NC form when irradiated at 446 nm. The DNA photocleavage activity of the complexes follows the order: **4–3** > **2** > **1**. The complexes also cleaved ~30–45% of supercoiled DNA to its nicked circular form when exposed to 660 nm laser radiation. The relatively lesser DNA photocleavage activity at 660 nm is probably due to lower extinction coefficient of the d-d bands of the copper complexes. The oxidative damage induced by the complexes correlates with the DNA binding affinity and photosensitizing ability of the complexes. Control experiments using Cu(II) salt, phen, dpq, dppz or aip ligand did not show any significant DNA photo-damage activity under similar experimental conditions. Therefore, the observed DNA photocleavage by the complexes **1–4** is believed to be Cu(II) assisted involving their d-d and charge transfer bands.

3.5. Photocytotoxicity study

Toxicities of the complexes **1–4** against HeLa (human cervical carcinoma) and MCF-7 (human breast adenocarcinoma) cancer cell lines in dark and visible light (400–700 nm) were evaluated using MTT, 3-(4,5-dimethylthiazol-2-yl)-2,5-diphenyltetrazolium bromide, assay (Figs. 3, Figs. S22–S24, Supplementary Information). A dose dependent cytotoxic activity of the complexes was observed against both HeLa and MCF-7 cells in dark as expected possibly due to the reduction of Cu(II) by cellular thiols and subsequent generation of radicals by Fenton type reaction. However, photo-irradiation with visible light (400–700 nm) resulted in significantly enhanced cytotoxicity of the complexes. A ~1.8–8 fold enhancement in the cytotoxicity of the complexes in HeLa cells was observed when exposed to visible light compared to the samples in dark. The aip complex **4** was found to be most toxic to HeLa cells with IC_{50} value of 3.24 μM when exposed to visible light. The IC_{50} values of the complexes tested, photofrin and cisplatin are listed in Table 3 [68–71]. The observed photocytotoxicity is comparable to that of photofrin. Cisplatin lacking any photoactive moiety showed an IC_{50} value of ~70 μM in both dark and light under similar experimental conditions. Control experiments with photo-exposure of the cells in

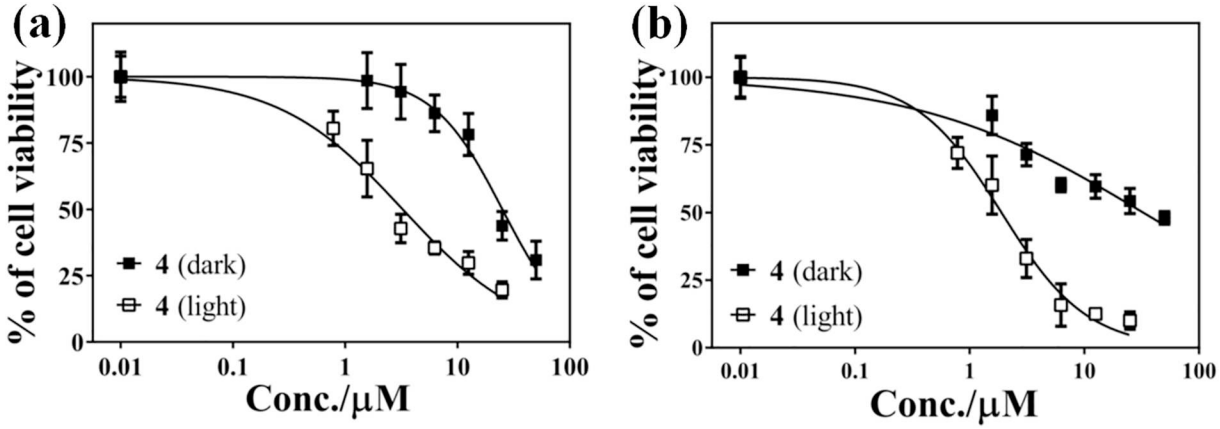

Fig. 3. Cell viability plots for the cytotoxic effect of complex **4** (50–0.78 μM) in (a) HeLa cells and (b) MCF-7 cells in dark (solid symbols) and in the presence of visible light (hollow symbols, 400–700 nm, 10 Jcm^{-2}). Each concentration of the complex was applied in triplicate.

Table 3
The IC_{50} values of Photofrin®, cisplatin, [Cu(Sal-Trp)(L)] (L = phen, **1**; dpq, **2**; dppz, **3**; nip, **4**) in HeLa and MCF-7 cells.[a]

Compound	HeLa		MCF-7	
	IC_{50} (μM) Dark[b]	IC_{50} (μM) visible light[c]	IC_{50} (μM) Dark[b]	IC_{50} (μM) visible light[c]
1	9.55 ± 1.59	5.40 ± 0.87	9.13 ± 1.40	3.92 ± 0.60
2	9.13 ± 1.62	3.92 ± 0.57	9.29 ± 1.89	2.80 ± 0.38
3	13.50 ± 3.07	3.64 ± 0.57	20.33 ± 5.50	2.15 ± 0.47
4	25.09 ± 4.04	3.24 ± 0.63	32.56 ± 3.05	1.89 ± 0.29
Photofrin®	> 41[d]	4.3 (± 0.2)[d]	–	2.0 (± 0.2)[e]
Cisplatin	71.3(± 2.9)[f]	68.7(± 3.4)[f]	[28.0(± 3.1)][g]	–

[a] The errors IC_{50} values are standard deviations of three experiments.
[b] The IC_{50} values correspond to 24 h incubation in dark.
[c] The IC_{50} values correspond to 4 h incubation in dark followed by photo-exposure to visible light (400–700 nm, 10 J cm^{-2}).
[d] The Photofrin® IC_{50} values (633 nm excitation; fluence rate: 5 J cm^{-2}) are taken from reference no. 68 (converted to μM using the approximate molecular weight of Photofrin®, 600 g M^{-1}).
[e] The Photofrin® IC_{50} values (2 h exposure; white bulb; fluence rate: 5.5 × 10^{-2} mW cm^{-2}) are taken from reference no 69.
[f] The IC_{50} values for 4 h treatment are taken from reference no 70.
[g] The IC_{50} value for 24 h treatment is taken from reference no 71.

absence of the complexes showed no apparent reduction in the cell viability. A similar photo-enhanced cytotoxic behavior of the complexes was seen on the breast cancer cell line (MCF-7) on exposure to visible light. Complex **4** was also found to be most cytotoxic towards MCF-7 cells giving IC_{50} of ~1.9 μM when exposed to visible light while remaining largely non-toxic in dark. Complexes were relatively more cytotoxic towards MCF-7 cells compared to the HeLa cells. The ligands or the metal salt were non-toxic both in dark and visible light (Table S3, Supplementary Information).

3.6. Measurement of lipophilicity

The passive partitioning into the cytoplasm from extracellular fluid through cell membrane is crucial for hydrophobic drugs [72,73]. A partition coefficient between *n*-octanol and water could be used to assess the ability of drug candidates to diffuse through lipid bilayer membrane of cells. To validate if the degree of lipophilicity in the complexes correlates with their in vitro photocytotoxicity in cancer cells, the *n*-octanol/water partition coefficients (expressed as log $P_{O/W}$) were determined and found to follow the order **4** > **3** > **2** > **1** (Table 2). The presence of flat planar extended aromatic groups along with the polar Sal-Trp ligand around the copper center is found to have large effect on the lipophilicity of the molecules. The data presented in Table 2 correlates with the photocytotoxicity of the complexes in HeLa and MCF-7 cancer cell lines. Complex **4** with highest lipophilic behavior is likely to pass through the lipid bilayer of cell most easily and show its activity upon activation by light. However, the higher photocytotoxicity of **3** and **4** could probably also be the result of higher photosensitizing ability of the respective phenanthroline ligands.

3.7. Cellular ROS generation

To evaluate the ability of the complexes to generate cellular ROS, DCFDA assay was performed [59,74]. H_2DCFDA or simply DCFDA is a non-fluorescent dye which forms H_2DCF by enzymatic reaction in intracellular fluid, which on oxidation by ROS generates fluorescent DCF with emission maximum at 528 nm [75]. HeLa cells were treated with complexes **1**–**4** (3 μM) in dark for 4 h and DCFDA (10 μM) for 30 min followed by 1 h incubation in dark or photo-exposure (400–700 nm) in DPBS and the assay was performed using flow cytometric analysis. A significant shift in the emission band towards right was shown by cells treated with complexes **1**–**4** upon light exposure indicates an increase in the intensity of emission resulting from the generation of DCF by the ROS-mediated oxidation of DCFDA (Fig. 4, Fig. S25, Supplementary Information). Careful analysis shows that the ability of formation of intracellular ROS correlates well with the IC_{50} values of complexes both in dark and light as listed in Table 3. Complex **4** exhibited maximum amount of ROS production after light exposure while remain most dormant in the dark conditions. The control experiments did not show any significant ROS formation while H_2O_2, the positive control, showed maximum production of ROS (Fig. S26, Supplementary Information).

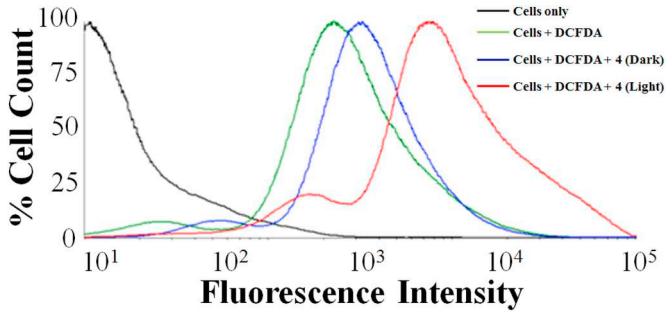

Fig. 4. Flow cytometry to detect the ROS generation using DCFDA assay for the complex **4** (3 μM) under different experimental conditions: cells only; cells + DCFDA; cells + DCFDA + complex **4** (in dark); and cells + DCFDA + complex **4** (in light). A greater shift in fluorescence intensity implies higher amount of DCF and greater ROS generation.

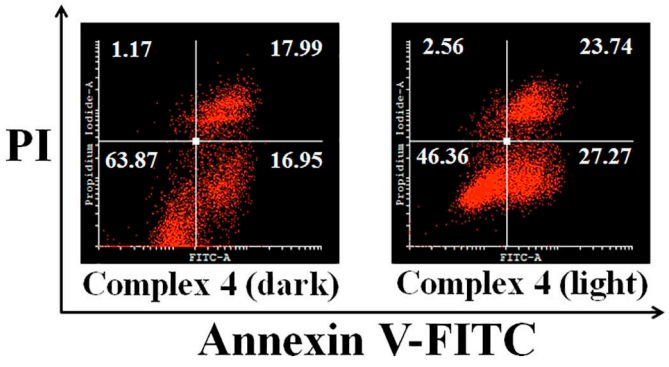

Fig. 5. FACScan profiles of Annexin V-FITC-PI staining of HeLa cells undergoing apoptosis induced by complex **4** (3 μM) in dark and visible light (400–700 nm).

The ROS generated by photoactivation of complexes **1**–**4** is believed to be responsible for the cell death.

3.8. FACScan analysis for mechanism of cell death

Cells undergoing apoptosis expresses phosphatidylserine on the outer surface of cells due to membrane flipping to which Annexin-V binds selectively. The ability of the copper complexes to induce apoptosis in HeLa cells was determined by treating the cancer cells with the most active complex **4** (3 μM) in dark as well as in visible light (400–700 nm) followed by staining with Annexin-V conjugated to FITC and propidium iodide (PI). Cells treated with **4** and exposed to visible light stained positive for Annexin-V due to membrane flipping which is one of the earliest events of apoptotic cell death. ~27% of the total cell population was in early stage of apoptosis showing positive Annexin-V staining whereas, the population of cells in late stage of apoptosis was ~24% (Fig. 5). The un-irradiated cells treated with **4** did not show significant apoptotic cell death compared to control experiment in dark (Fig. S27, Supplementary Information). These results clearly show that the complex **4** is capable of inducing significant apoptotic cell death on photo-activation.

3.9. Confocal imaging

Complex **4** bearing a fluorescent anthracenyl moiety is designed and synthesized for cellular imaging using confocal microscopy to study its uptake and localization in the HeLa (Fig. 6, panels A–D) and MCF-7 (Fig. 6, panels E–H) cells. HeLa cells, on treatment with complex **4** (5 μM) for a time period of 4 h, were observed to show predominant cytosolic localization as evident from the blue fluorescence (Fig. 6, panel B). Complex **4** (5 μM) displayed similar cellular localization behavior in MCF-7 cells as well (Fig. 6, panel F). The cells were co-stained with propidium iodide (PI) which stains only the nucleus in presence of RNase which degrades the cellular RNA (Fig. 6, panels A and E). The merged images (panels C and G) clearly indicate cytosolic localization of complex **4** in both the cancer cell lines. The bright field images are shown in panels D and H.

4. Conclusion

Four ternary copper(II) complexes containing a reduced Schiff base ligand derived from L-Tryptophan and salicylaldehyde and phenanthroline bases were synthesized, fully characterized and their cytotoxicity, mechanism of cell death and cellular localization studied in cancer cells. The rationale of the design of the complexes is to attach the *N*-Salicylyl-L-Tryptophan ligand into a Cu(II) center which is further bound to a phenanthroline base which serves the dual purpose of DNA binder and photosensitizer. The complexes exhibit efficient binding propensity to CT DNA probably through partial intercalation. They photo-cleave pUC19 DNA in visible laser light of 446 and 660 nm. The complexes are remarkably cytotoxic towards cervical (HeLa) and breast (MCF-7) cancer cells on exposure to low energy visible light. Significant induction of apoptosis is observed in photo-irradiated HeLa cells pretreated with complex **4**. The fluorescence emission of complex **4** bearing an anthracenyl moiety is exploited for confocal imaging which shows primary cytosolic localization in both HeLa and MCF-7 cells. The present investigation of optimally lipophilic copper(II) complexes having biocompatible ligands as efficient photocytotoxic agents opens up new directions towards the development of 3d-metal based antitumor drugs.

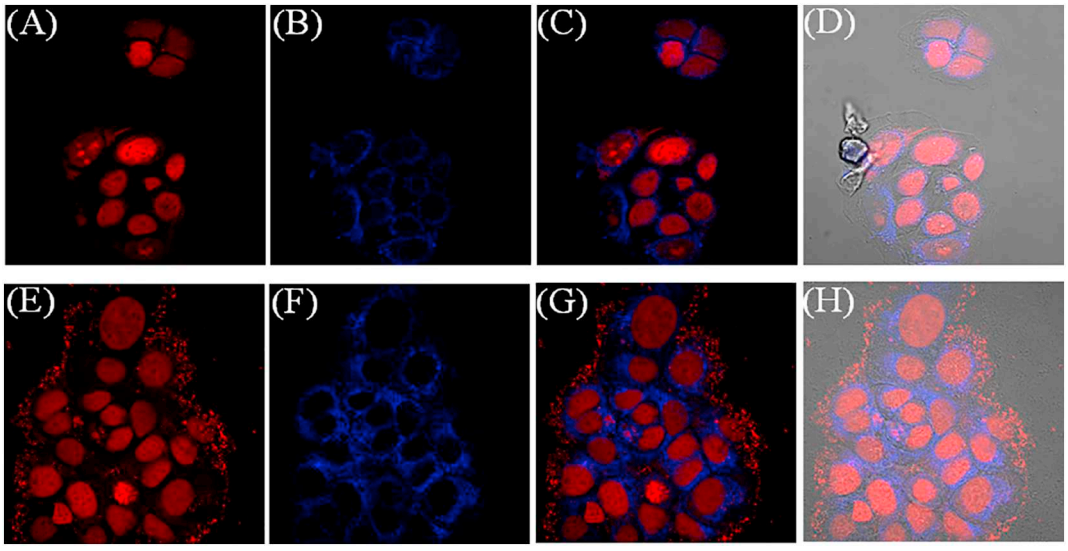

Fig. 6. Confocal microscopic images of HeLa (panels A to D) and MCF-7 (panels E to H) cells treated with complex **4** (5 μM) for 4 h and propidium iodide (PI). Panels (B) and (F) correspond to the blue emission of complex **4** upon excitation with 405 nm laser. Panels (A) and (E) correspond to the red emission of PI. Panels (C) and (G) are the merged images of the first two panels and (D) and (H) are the bright field images respectively. The scale bar in panel (a) corresponds to 20 μm. (For interpretation of the references to color in this figure legend, the reader is referred to the web version of this article.)

Acknowledgments

The authors thank the Department of Science and Technology (DST) INSPIRE Program, Government of India, for financial support (IFA14-CH-164). We are thankful to DST and Department of SAIF, Gauhati University for a CCD diffractometer facility. We also thank Dr. Ranjit Thakuria and Dr. Sanjib Karmakar for helping with X-ray crystallographic procedures. The authors are grateful to Ms. Aida Jameei, Department of Biochemistry, Indian Institute of Science, Bangalore for helping in the biological assays and Prof. Anjali A. Karande, Department of Biochemistry, Indian Institute of Science, Bangalore for allowing us to use the cellular facilities in her laboratory. We thankfully acknowledge the supports of Bio-imaging and the flow cytometry facility of Division of Biological Sciences, Indian Institute of Science. AB thanks DST INSPIRE, New Delhi, for research fellowship. AB* thanks Council of Scientific and Industrial Research (CSIR), New Delhi, for research fellowship.

Appendix A. Supplementary data

CIF file giving crystallographic data for complex **1**, selected bond distance and bond angle for complex **1** (Table S1), DNA and protein binding constants (Table S2), cytotoxicity data (Table S3), synthetic schemes (S1, S2) and figures showing mass spectra of ligand and the complexes (S1, S7–S10), UV–visible spectra for stability measurements (S4–S6), IR spectra (S2, S11–S14), ligand ^{1}H NMR spectra (S3), fluorescence spectrum (S15), cyclic voltammograms (S16), unit cell packing diagram (S17), DNA binding plots (S18), protein binding plots (S19, S20), gel figures for DNA cleavage experiments (S21), cytotoxicity data (S22–S27). Supplementary data to this article can be found online at https://doi.org/10.1016/j.jinorgbio.2018.11.005.

References

[1] H.-K. Liu, P.J. Sadler, Acc. Chem. Res. 44 (2011) 349–359.
[2] A. Bergamo, G. Sava, Dalton Trans. 40 (2011) 7817–7823.
[3] N.J. Wheate, S. Walker, G.E. Craig, R. Oun, Dalton Trans. 39 (2010) 8113–8127.
[4] A. Bergamo, C. Gaiddon, J.H.M. Schellens, J.H. Beijnen, G. Sava, J. Inorg. Biochem. 106 (2012) 90–99.
[5] T.W. Hambley, Science 318 (2007) 1392–1393.
[6] A. Casini, J. Inorg. Biochem. 109 (2012) 97–106.
[7] Y. Yan, J. Zhang, L. Ren, C. Tang, Chem. Soc. Rev. 45 (2016) 5232–5263.
[8] M. Zaki, F. Arjmand, S. Tabassum, Inorg. Chim. Acta 444 (2016) 1–22.
[9] R.W. Sun, D. Ma, E.L. Wong, C. Che, Dalton Trans. (2007) 4884–4892.
[10] F. Li, G. Collins, F.R. Keene, Chem. Soc. Rev. 44 (2015) 2529–2542.
[11] C.S. Allardyce, P.J. Dyson, Dalton Trans. 45 (2016) 3201–3209.
[12] P.J. Dyson, G. Sava, Dalton Trans. (2006) 1929–1933.
[13] R. Bonnett, Chemical Aspects of Photodynamic Therapy, Gordon & Breach, London, U.K., 2000.
[14] N.L. Fry, P.K. Mascharak, Acc. Chem. Res. 44 (2011) 289–298.
[15] A.M. Bugaj, Photochem. Photobiol. Sci. 10 (2011) 1097–1109.
[16] M. Ethirajan, Y. Chen, P. Joshi, R.K. Pandey, Chem. Soc. Rev. 40 (2011) 340–362.
[17] D. Crespy, K. Landfester, U.S. Schubert, A. Schiller, Chem. Commun. 46 (2010) 6651–6662.
[18] A.P. Castano, P. Mroz, M.R. Hamblin, Nat. Rev. Cancer 6 (2006) 535–545.
[19] S.I. Moriwaki, J. Misawa, Y. Yoshinari, I. Yamada, M. Takigawa, Y. Tokura, Photodermatol. Photoimmunol. Photomed. 17 (2001) 241–243.
[20] M. Ochsner, J. Photochem. Photobiol. B 32 (1996) 3–9.
[21] N.J. Farrer, L. Salassa, P.J. Sadler, Dalton Trans. (2009) 10690–10701.
[22] C. Mari, V. Pierroz, A. Leonidova, S. Ferrari, G. Gasser, Eur. J. Inorg. Chem. (2015) 3879–3891.
[23] U. Schatzschneider, Eur. J. Inorg. Chem. (2010) 1451–1467.
[24] K. Mitra, Dalton Trans. 45 (2016) 19157–19171.
[25] A. Naik, R. Rubbiani, G. Gasser, B. Spingler, Angew. Chem. 126 (2014) 7058–7061.
[26] F.S. Mackay, J.A. Woods, P. Heringová, J. Kašpárková, A.M. Pizarro, S.A. Moggach, S. Parsons, V. Brabec, P.J. Sadler, Proc. Natl. Acad. Sci. U. S. A. 104 (2007) 20743–20748.
[27] A.M. Angeles-Boza, H.T. Chifotides, J.D. Aguirre, A. Chouai, P. K, L. Fu, K.R. Dunbar, C. Turro, J. Med. Chem. 49 (2006) 6841–6847.
[28] U. Bhattacharyya, B. Kumar, A. Garai, A. Bhattacharyya, A. Kumar, S. Banerjee, P. Kondaiah, A.R. Chakravarty, Inorg. Chem. 56 (2017) 12457–12468.
[29] H. Yin, M. Stephenson, J. Gibson, E. Sampson, G. Shi, T. Sainuddin, S. Monro, S.A. McFarland, Inorg. Chem. 53 (2014) 4548–4559.
[30] Y. Zheng, L. He, D. Zhang, C. Tan, L. Ji, Z. Mao, Dalton Trans. 46 (2017) 11395–11407.
[31] J. Wang, Y. Lu, N. McGoldrick, C. Zhang, W. Yang, J. Zhao, S.M. Draper, J. Mater. Chem. C 4 (2016) 6131–6139.
[32] R.E. Doherty, I.V. Sazanovich, L.K. McKenzie, A.S. Stasheuski, R. Coyle, E. Baggaley, S. Bottomley, J.A. Weinstein, H.E. Bryant, Sci. Rep. 6 (22668) (2016) 1–9.
[33] P.K. Sasmal, A.K. Patra, M. Nethaji, A.R. Chakravarty, Inorg. Chem. 46 (2007) 11112–11121.
[34] P.R. Reddy, A. Shilpa, N. Raju, P. Raghavaiah, J. Inorg. Biochem. 105 (2011) 1603–1612.
[35] T.K. Goswami, S. Gadadhar, B. Balaji, B. Gole, A.A. Karande, A.R. Chakravarty, Dalton Trans. 43 (2014) 11988–11999.
[36] T.K. Goswami, S. Gadadhar, B. Gole, A.A. Karande, A.R. Chakravarty, Eur. J. Med. Chem. 63 (2013) 800–810.
[37] T.K. Goswami, M. Roy, M. Nethaji, A.R. Chakravarty, Organometallics (28) (2009) 1992–1994.
[38] A. Bhattacharyya, A. Dixit, K. Mitra, S. Banerjee, A.A. Karande, A.R. Chakravarty, Med. Chem. Commun. 6 (2015) 846–851.
[39] A. Bhattacharyya, A. Dixit, S. Banerjee, B. Roy, A. Kumar, A.A. Karande, A.R. Chakravarty, RSC Adv. 6 (2016) 104474–104482.
[40] A. Bhattacharyya, A. Jameei, A. Garai, R. Saha, A.A. Karande, A.R. Chakravarty, Dalton Trans. 47 (2018) 5019–5030.
[41] K. Mitra, S. Gautam, P. Kondaiah, A.R. Chakravarty, ChemMedChem 11 (2016) 1956–1967.
[42] M.K. Raza, S. Gautam, A. Garai, K. Mitra, P. Kondaiah, A.R. Chakravarty, Inorg. Chem. 56 (2017) 11019–11029.
[43] W.W. Souba, A.J. Pacitti, J. Parenter. Enter. Nutr. 16 (1992) 569–578.
[44] J.E. Dickeson, L.A. Summers, Aust. J. Chem. 23 (1970) 1023–1027.
[45] E. Amouyal, A. Homsi, J.-C. Chambron, J.-P. Sauvage, J. Chem. Soc. Dalton Trans. (1990) 1841–1845.
[46] M. Mariappan, B.G. Maiya, Eur. J. Inorg. Chem. (2005) 2164–2173.
[47] O. Kahn, Molecular Magnetism, VCH, Weinheim, 1993.
[48] A.K. Renfrew, Metallomics 6 (2014) 1324–1335.
[49] N. Walker, D. Stuart, Acta Crystallogr. Sect. A 39 (1983) 158–166.
[50] G.M. Sheldrick, Acta Cryst A64 (2008) 112–122.
[51] L.J. Farrugia, J. Appl. Crystallogr. 30 (1997) 565.
[52] T.K. Goswami, B.V.S.K. Chakravarthi, M. Roy, A.A. Karande, A.R. Chakravarty, Inorg. Chem. 50 (2011) 8452–8464.
[53] J.D. McGhee, P.H. Von Hippel, J. Mol. Biol. 86 (1974) 469–489.
[54] J. Seetharamappa, B.P. Kamat, Chem. Pharm. Bull 52 (2004) 1053–1057.
[55] F.M. Ausubel, R. Brent, R.E. Kingston, D.D. Moore, J.G. Seidman, J.A. Smith, K. Struhl, Current Protocols in Molecular Biology, John Wiley & Sons, 2003.
[56] J. Bernadou, G. Pratviel, F. Bennis, M. Girardet, B. Meunier, Biochemistry 28 (1989) 7268–7275.
[57] T. Mosmann, J. Immunol. Methods 65 (1983) 55–63.
[58] J. Wu, D.G.J. Goodwin, K. Peter, D. Benoit, W. Li, D.H. Fairbrother, J.D. Fortner, Environ. Sci. Technol. Lett. 1 (2014) 490–494.
[59] E. Eruslanov, S. Kusmartsev, Advanced Protocols in Oxidative Stress II, (2009), pp. 57–72.
[60] C. Soni, A.A. Karande, Mol. Immunol. 47 (2010) 2458–2466.
[61] J.L. McClintock, B.P. Ceresa, Invest. Opthalmol. Vis. Sci. 51 (2010) 3455–3461.
[62] T.K. Goswami, S. Gadadhar, M. Roy, M. Nethaji, A.A. Karande, A.R. Chakravarty, Organometallics 31 (2012) 3010–3021.
[63] O. Mazuryk, K. Magiera, B. Rys, F. Suzenet, C. Kieda, M. Brindell, J. Biol. Inorg. Chem. 19 (2014) 1305–1316.
[64] S. Dhar, D. Senapati, P.K. Das, P. Chattopadhyay, M. Nethaji, A.R. Chakravarty, J. Am. Chem. Soc. 125 (2003) 12118–12124.
[65] A.M. Pyle, J.P. Rehmann, R. Meshoyrer, C.V. Kumar, N.J. Turro, J.K. Barton, J. Am. Chem. Soc. 111 (1989) 3051–3058.
[66] M.J. Hawkins, P. Soon-Shiong, N. Desai, Adv. Drug Deliv. Rev. 60 (2008) 876–885.
[67] B.P. Espósito, R. Najjar, Coord. Chem. Rev. 232 (2002) 137–149.
[68] E. Delaey, F. Van Larr, D. De Vos, A. Kamuhabwa, P. Jacobs, P. De Witte, J. Photochem. Photobiol. B 55 (2000) 27–36.
[69] F. Ménard, V. Sol, C. Ringot, R. Granet, S. Alves, C.L. Morvan, Y. Queneau, N. Ono, P. Krausz, Bioorg. Med. Chem. 17 (2009) 7647–7657.
[70] S. Saha, D. Mallick, R. Majumdar, M. Roy, R.R. Dighe, E.D. Jemmis, A.R. Chakravarty, Inorg. Chem. 50 (2011) 2975–2987.
[71] A.R. Ghezzi, M. Aceto, C. Cassino, E. Gabano, D. Osella, J. Inorg. Biochem. 98 (2004) 73–78.
[72] I. Kos, J.S. Rebouças, G. Defreitas-Silva, D. Salvemini, Z. Vujaskovic, M.W. Dewhirst, I. Spasojević, I. Batinić-Haberle, Free Radic. Biol. Med. 47 (2009) 72–78.
[73] S. Mukhopadhyay, R.S. Singh, R.P. Paitandi, G. Sharma, B. Koch, D.S. Pandey, Dalton Trans. 46 (2017) 8572–8585.
[74] T. Ohashi, A. Mizutani, A. Murakami, S. Kojo, T. Ishii, S. Taketani, FEBS Lett. 511 (2002) 21–27.
[75] T. Takanashi, Y. Ogura, H. Taguchi, M. Hashizoe, Y. Honda, Invest. Ophthalmol. Vis. Sci. 38 (1997) 2721–2728.